ENABLING POLY ETHER ETHER KETONE AS A SOLID POLYMER ELECTROLYTE FOR STRUCTURAL BATTERY COMPOSITES

Mia R. Carrola[1], Amir Asadi[2], Ahmad Amiri[3], Zhenning Yu[4], Hilmar Koerner[1]
1- Air Force Research Laboratory
WPAFB, OH/USA
2- Texas A&M University
College Station, TX/USA
3- University of Tulsa
Tulsa, OK/USA
4- BlueHalo LLC
Dayton, OH/USA

ABSTRACT

To advance the state of structural battery composites, more mechanically robust polymeric materials must be investigated for use as the ionically conductive electrolyte. Currently, the matrices being utilized in solid polymer electrolytes lack mechanical strength, and are often gels, due to their amorphous structure offering increased lithium-ion conductivity. To address the need for more robust, semicrystalline polymer matrices, poly ether ether ketone (PEEK) was selected as a candidate that would offer both ionic conductivity and mechanical reinforcement in these novel multifunctional composite structures. Through a series of functionalization procedures, specifically sulfonation and lithiation of the polymer chains, the PEEK exhibits ionic conductivity and an amorphous microstructure. However, to maintain the structural characteristics required of the matrix, careful functionalization is used to tailor the PEEK electrolytes and strike a balance between the two inversely related properties (ion conductivity and crystallinity). It was found that selective adjusting of the morphology of the solid electrolyte successfully enables the two properties that are most important for this multifunctional application. The discoveries presented from this work provide a foundation to continue progress on thermoplastic structural battery composites.

Keywords: structural battery composite, solid polymer electrolyte, polyelectrolyte, polyether ether ketone, additive manufacturing
Corresponding author: Mia Carrola, Email: mia.carrola.2@us.af.mil

1. INTRODUCTION

As the demand for battery technology strengthens, both with the exponential rise in popularity of electric vehicles (EVs) and handheld, portable electronics, there is a requirement to improve the current state of battery technology. The lithium-ion battery, first introduced by Sony nearly 35 years ago, revolutionized portable energy storage and brought it to commercial markets and the hands of consumers [1]. In the decades following, research in the field of lithium-ion batteries exponentially increased, with efforts to improve the safety of the cells, increase the lifespan and performance, and investigate how to decrease the dimensions and weight while maintaining

SAMPE Conference Proceedings. Indianapolis, IN, May 19-22, 2025. Society for the Advancement of Material and Process Engineering – North America.

(DOI will be added by SAMPE)

current energy storage capabilities. Though many advancements have materialized in the form of cathode and anode materials, one technology, structural battery composites, threatens to revolutionize the way that energy storage is utilized moving forward.

Structural battery composites, SBCs, are a massless energy storage alternative to the traditional lithium-ion cells. In SBCs, each constituent acts as a multifunctional material, acting both as an energy storage cell and a structural component [2-6]. These composites are typically made of a carbon fiber anode, polymer-based solid electrolyte, and coated carbon fiber cathode, as shown in **Figure 1**. The carbon fibers fulfill many roles, including mechanical reinforcement for the composite structure, electrode in the battery cell, and as a current collector. The SBCs hold much promise for light-weighting aircraft such as unmanned aerial vehicles (UAVs) and consumer EVs, providing higher efficiency and longer distances travelled on a single charge [7]. To realize this technology, the materials comprising the structure must first be investigated and optimized, specifically in the case of the solid polymer electrolyte. Arguably, the biggest obstacle that is faced with polymer electrolytes is balancing the ionic conductivity and crystallinity, which have an inverse relationship. As the crystallinity in the polymer increases, often its strength and stiffness increase, while the restricted chain motion in this type of morphology is not conducive for lithium ions to conduct through. Amorphous polymers are therefore preferable to semicrystalline options for increased ionic conductivity, though the mechanical properties can be compromised. One of the most prominent materials currently used as a solid polymer electrolyte is polyethylene oxide (PEO), due to its notable ionic conductivity, ranging from 10^{-7} to 10^{-2} $S \cdot cm^{-1}$, depending on the lithium salt that was used in the system [8]. These materials are largely amorphous, leading to lowered mechanical strength for resultant SBCs, with some tensile strengths reaching a maximum of only 3.5 MPa [10].

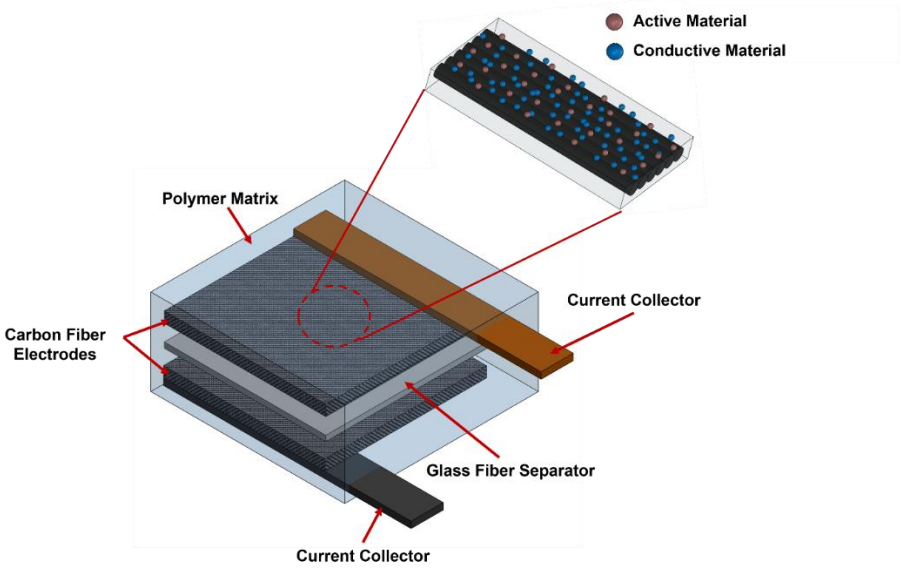

Figure 1*: Schematic of structural battery composite layup, including carbon fiber woven fabric acting as the anode, a cathode consisting of woven carbon fiber fabric coated with active and conductive materials, a glass fiber separator, a polymer matrix that can serve as a solid polymer electrolyte, and two current collectors.*

To address the current knowledge and materials gap in the solid polymer electrolyte space, polyether ether ketone (PEEK) was selected as the basis for creating an ionically conductive polymer that retains its properties as a high-performance thermoplastic material. PEEK is known for its thermal stability at elevated temperatures, its chemical inertness, and its strength [10, 11]. This makes it an excellent choice for various engineering applications, including in carbon fiber reinforced composites, through pre-preg fabrics and tapes that can be utilized in various manufacturing applications [12, 13].

It has been shown that PEEK's morphology can be tailored through several methods, including using carbonaceous nanomaterials and other additives, post-process annealing, and even additive manufacturing techniques [14-17]. Leveraging this knowledge of methods for tailoring morphology, it is hypothesized that the material can therefore be an ideal candidate for creating an architecture that is both ionically conductive and maintains structural integrity. This work utilizes additive manufacturing and functionalization methodology to impart tailored microstructure into a solid PEEK electrolyte, creating a multifunctional material that is promising for the future of structural battery composites.

2. EXPERIMENTATION

2.1 Materials

Neat PEEK pellets that were used for sulfonation and lithiation processes are Arlon 1000, supplied by Greene Tweed (USA), 96% ACS Grade sulfuric acid was obtained from Fisher Scientific. Anhydrous lithium hydroxide (LiOH) was furnished by Sigma Aldrich.

2.2 Sulfonation and Lithiation Methodology

2.2.1 Sulfonation of PEEK

PEEK pellets were sulfonated using 50 g of Arlon 1000 that were dried in an oven at 100 °C overnight. Following this, 1 L of sulfuric acid was added to a round bottom flask that was equipped with a stir bar in an oil bath. The acid was heated to 50 °C and stirred at 200 rpm before the PEEK pellets were slowly added to the flask. The PEEK pellets were stirred at 50 °C for 96 hours, until they were completely dissolved. At this point, the PEEK was then precipitated out into abundant DI water dropwise. The resultant sulfonated PEEK (S-PEEK) precipitate was then filtered with DI water until a pH level of ~5 was achieved.

2.2.2 Surface Sulfonation of Printed PEEK

Surface sulfonation of printed PEEK disks was achieved with a similar methodology. Approximately 25 mL of sulfuric acid was added to a petri dish and placed onto a hot plate where it was heated to 50 °C. To this, the printed PEEK disk was added, careful not to fully submerge the sample in the sulfuric acid. After 3 minutes on the initial side, the PEEK disk was flipped to the unfunctionalized side and kept in the acid for 3 minutes. Following the surface sulfonation on both sides of the disk, the disk was placed into 100 mL of DI water for 5 minutes before being extracted and dried in an oven at 60 °C.

2.2.3 Lithiation of PEEK

PEEK was lithiated using a 1M solution of LiOH in DI water, based on the method presented by Li et al [18]. S-PEEK was placed into the 1M LiOH solution, following the sulfonation procedure, and stirred until the pH of the solution was very alkaline (pH~12). Following this step, the lithiated PEEK (Li-PEEK) was filtered using DI water until a pH of approximately 5 was reached.

2.3 Fused Filament Fabrication (FFF) and Sample Manufacturing

Neat PEEK meshes were printed using a Hyrel System 30M equipped with an FH2-450 print head and heated print bed with a GeckoTek EZStik Hot substrate. The nozzle used was 0.5 mm in diameter set to a temperature of 400 °C and the print bed to 75 °C, using a printing speed of 10 mm/s. Prusa Slic3r was used to create the G Code files for each mesh using four different patterns: grid, honeycomb, triangle, and 3D honeycomb. Each of the meshes consisted of two layers 0.2 mm in height. Annealed meshes were placed into a 30 °C oven and heated to 100 °C, soaked for 1 hour and then slow-cooled until they reached 30 °C.

Functionalized (S-PEEK and Li-PEEK) PEEK was introduced to the neat PEEK meshes using a Wabash 30 Ton Heated Press at a temperature of 150 °C and pressure of approximately 1000 ft.lbs, held for 90 seconds at pressure. The meshes were prepared for pressing by adding crushed pieces of S-PEEK onto the mesh before pressing.

2.4 Material Characterization Methodology

2.4.1 ^{1}H NMR

Proton ^{1}H nuclei magnetic resonance (NMR) spectra were acquired on a Bruker NMR spectrometer (Bruker Corporation, Billerica, MA), with Ascend 400 magnet and AVANCE NEO Console, operating at 400.23 MHz for proton spectrum acquisition. Samples were dissolved in 99.8% deuterated dimethyl sulfoxide (DMSO-d_6). NMR tests were completed at room temperature.

2.4.2 Thermogravimetric Analysis (TGA)

Thermogravimetric analysis (TGA) was performed using the TGA Discovery 5500 (TA Instruments). Each sample was run from 30 °C to 1000 °C at a heating rate of 10°C/min in both air and nitrogen atmospheres to evaluate the thermal stability of functionalized PEEK.

2.4.3 Dynamic Mechanical Analysis (DMA)

Dynamic mechanical analysis (DMA) tests were conducted using the DMA Discovery 850 (TA Instruments). For all tests, the thin film fixture was used in tensile mode. The experiments were performed in air under a constant frequency of 1 Hz and an oscillating amplitude of 5 μm. To evaluate the mechanical response as a function of temperature, a temperature ramp from 35 °C to 175 °C at a rate of 2 °C/min was utilized. All samples were prepared according to recommendations from TA Instruments, having standard dimensions of 30 mm × 5 mm × 0.5 mm.

2.4.4 Wide Angle and Small Angle X-Ray Scattering

Wide-angle and medium- angle X-ray scattering patterns were acquired using the Xenocs (Holyoke, MA, USA) Xuess 3.0 X-Ray scattering system. The Xuess is equipped with a Dectris Eiger 2R 1M-pixel detector and a Genix 3D X-ray beam delivery system, which produces a monochromatic Cu Ka high intensity X-ray beam. The collected 2D scattering patterns were reduced into 1D plots and analyzed using XSACT software.

2.4.5 Microbeam and X-Ray Fluorescence

Microbeam and X-ray fluorescence (XRF) experiments were conducted at the Functional Materials Beamline (FMB) of the Materials Solutions Network at the Cornell High Energy Synchrotron Source (MSN-C). These studies were conducted in microprobe mode[22] with an X-ray beam energy of 9.7 keV (λ = 0.128 nm) and incident flux of $\approx 2 \times 10^{10}$ photons/s focused to area of $\approx 3 \times 15$ μm^2. The wide angle X-ray scattering (WAXS) data were collected using two, two-dimensional (2D) detectors (model Pilatus3 200K, Dectris AG, Baden-Daettwil, Switzerland). The XRF setup at FMB used a 384-element Maia x-ray fluorescence (XRF) detector, developed by BNL and CSIRO, was used to collect XRF spectra [19].

3. RESULTS

3.1 Functionalized PEEK Constituents

3.1.1 Degree of Sulfonation

During the sulfonation treatment, the PEEK backbone has a sulfonic acid group (SO_3H) introduced to one of the aromatic rings, as depicted in **Figure 2**. This sulfonic acid group provides a vehicle for the second step of functionalization, lithiation, where the material is neutralized with LiOH to form SO_3Li groups. This method for functionalization allows for higher ionic conductivity, according to literature. To confirm the degree of sulfonation, corresponding to the percentage of polymer chains that have the sulfonic acid group introduced to the backbone, ^{1}NMR was used. The ^{1}NMR spectra of S-PEEK samples after filtering is shown (**Figure 2c**). The peaks that occur at 7.25 ppm represent the C protons in the PEEK repeat unit (**Figure 2b**). When the sulfonic acid group is attached to the aromatic ring, the protons are differentiated into C, D, and E, Figure 2b. The degree of sulfonation (DS) can be determined by evaluating the peak area represented by the protons at the positions of A and A', as the molar ratio of these protons is determined to be $4I_E/I_{AA'}$. In **Figure 2c**, the NMR spectra exhibits an additional peak at 7.95 ppm, corresponding to what is hypothesized as free sulfuric acid in the sample. From the spectra, it is determined that the DS achieved with the aforementioned method is approximately 96%.

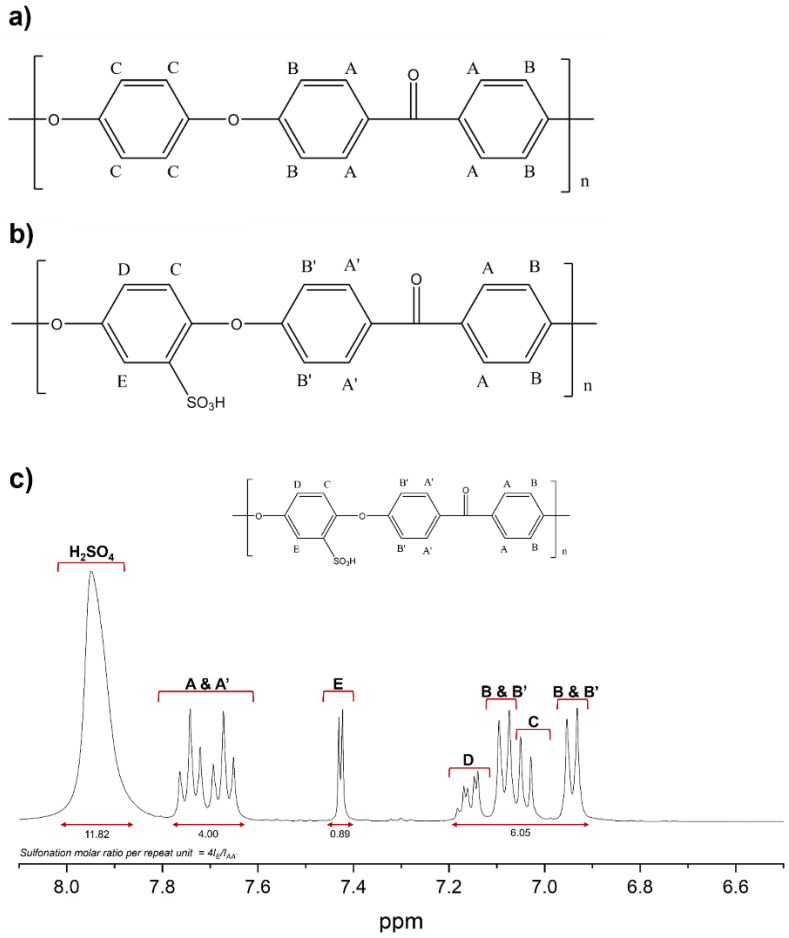

***Figure 2**: PEEK chain **a)** before and **b)** after sulfonation treatment, with sulfonic acid group attached to an aromatic ring on the backbone. **c)** NMR spectra exhibiting sulfonic acid groups on the PEEK chain.*

3.1.2 Thermal Stability

The thermal stability of the functionalized PEEK (both sulfonated and lithiated) was evaluated using TGA scans in air and nitrogen environments, to examine the effects of the processing conditions on the material (**Figure 3a**). Neat PEEK, used as a control, withstands temperatures of nearly 600 °C before degradation begins in both air and nitrogen. Before this point, the material maintains thermal stability at elevated temperatures. On the contrary, the S-PEEK shows several distinct degradation behaviors as temperatures reach up to 1000 °C. Between temperatures of 30 °C to 150 °C, any excess water present in the hygroscopic material is evaporated, leading to the first weight loss curve shown in **Figure 3b**. Above 150 °C until approximately 400 °C, there is a secondary weight loss that occurs, hypothesized to reflect the degradation of the sulfonic acid groups that were introduced during the sulfonation process. During this de-sulfonation process, the sulfonic acid groups decompose into H_2O and SO_2, resulting in PEEK chains that are no longer functionalized. In fact, this second weight loss can be used to estimate the degree of sulfonation of the S-PEEK [20]. The final weight loss peak in the S-PEEK curve corresponds to the degradation

of the PEEK polymer chains, which becomes most prevalent at the same temperature of neat PEEK, approximately 600 °C.

Li-PEEK displays a thermal stability behavior that suggests a combination of those displayed by neat PEEK and S-PEEK, where there is water evaporation present and some degradation of the functional groups, however it appears to be more stable at higher temperatures than its S-PEEK counterpart. In air, the functional Li group appears to begin degradation at nearly 500 °C, followed by the degradation of the PEEK polymer chains around 600 °C. With the weight loss of the material reaching only ~10% at 500 °C, this finding suggests that the Li-PEEK is thermally stable in elevated temperatures, which are often encountered during the operation of a LIB cell.

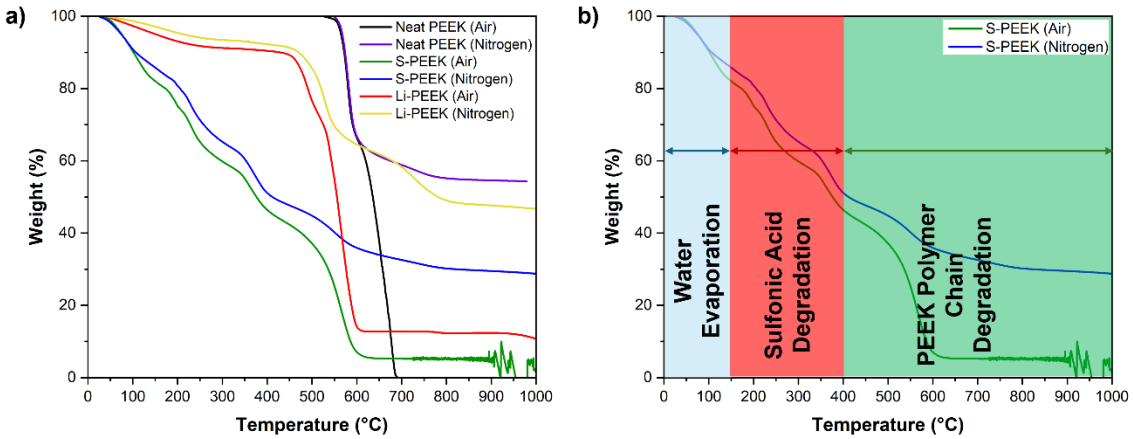

Figure 3: a) *Thermal stability of neat PEEK, sulfonated PEEK (S-PEEK), and lithiated PEEK (Li-PEEK) in nitrogen and air environments from ambient temperature to 1000 °C.* ***b)*** *Labelled thermal decomposition of S-PEEK including weight loss peaks corresponding to the water evaporation, sulfonic acid group degradation, and, finally, the degradation of PEEK polymer chains.*

3.1.3 Crystalline and Amorphous Behaviors

To characterize the morphology of each of the PEEK constituents, wide-angle and medium-angle x-ray scattering was performed, shown in **Figure 4**. The annealed PEEK (red) is shown to be the only PEEK based sample that displayed crystalline peaks in the reduced 1D wide angle scattering data (**Figure 4a**) and a distinct semi-crystalline peak in the medium angle scattering plot (**Figure 4b).** The as-printed neat PEEK shows a completely amorphous behavior, without any notable crystalline peaks in either scattering angle. However, both functionalized PEEK derivatives, S-PEEK and Li-PEEK show similar amorphous microstructures, with no crystalline peaks exhibited. The unique feature of the functionalized PEEK lies in what is known as the ionomer peak, present at q values of approximately 0.35 $Å^{-1}$. The ionomer peak is indicative of a polyelectrolyte material, and can suggest that the material is ionically conductive. The normalized intensity of the ionomer peak is less in the S-PEEK than in the Li-PEEK, which implies that the lithiation treatment is a necessary step to achieve not only an amorphous phase within the polymer, but also an optimized ionomer peak, which can lead to higher ionic conductivity.

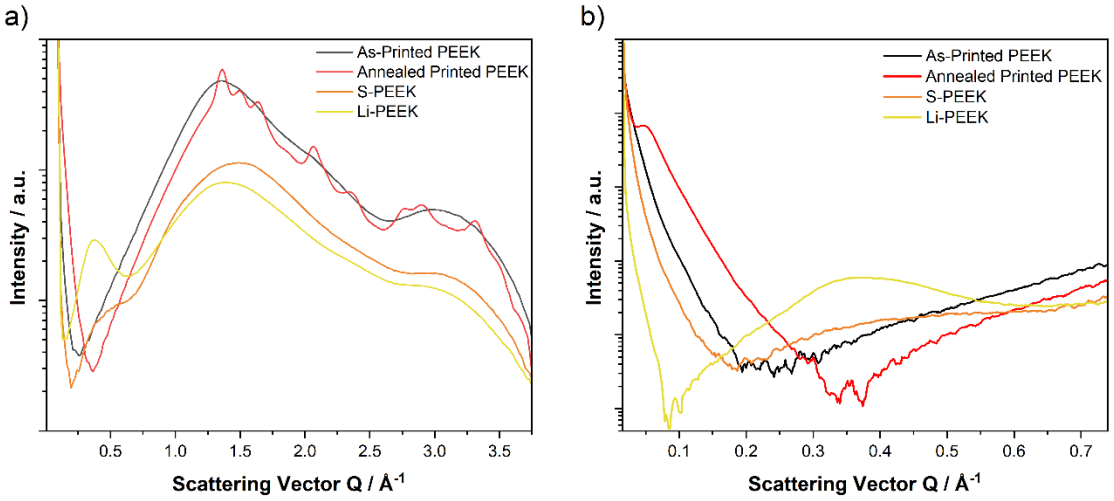

Figure 4: a) *Wide angle and* ***b)*** *medium angle x-ray scattering patterns of neat PEEK, annealed PEEK, sulfonated PEEK (S-PEEK), and lithiated PEEK (Li-PEEK) showing crystallinity in annealed PEEK and an ionomer peak in both functionalized PEEK samples (S-PEEK, Li-PEEK) at q= 0.35 Å^{-1}.*

3.1.4 Thermomechanical Properties

The thermomechanical properties of the neat PEEK, annealed neat PEEK, and functionalized PEEK were evaluated in temperatures ranging from ambient to 175 °C, in order to understand the behavior of the materials under various temperatures, which can be expected in the lithium-ion structural battery cell. The storage modulus, which is related to the material's elastic response to stress and is an indicator of its stiffness, can be seen in **Figure 5a**. With the printed neat PEEK (black) as the baseline for the rest of the samples, the storage modulus gradually decreases from 1120 MPa at ambient temperature to less than 100 MPa above the glass transition temperature (T_g), as it becomes transitions into the rubbery state from the glassy state. The annealed printed PEEK showed a similar behavior, with a higher storage modulus overall, peaking at values of just under 1200 MPa (1179 MPa), with the transition from the glassy to the rubbery state occurring at a higher temperature, closer to 150 °C. Though there is not much difference between these two samples, the functionalized PEEK, both S-PEEK and Li-PEEK, display much different behaviors. S-PEEK initially has a higher storage modulus at ambient temperature (1367.7 MPa) than that of its neat PEEK counterparts, while it does display a steeper decline of this property at lower temperatures, just above 100 °C. Conversely, the lithiated PEEK displays a lower value for the storage modulus (862 MPa), indicating lower stiffness in the material, but maintains the storage modulus at temperatures up to and including 175 °C. The thermal stability of the Li-PEEK material was demonstrated in the TGA analysis and continues to prove a higher stability than that of its neat PEEK counterparts, suggesting that it is a promising alternative for traditional liquid electrolytes and a viable option for use in structural battery composites.

The loss modulus, shown in **Figure 5b**, displays the materials' ability to dissipate energy as heat and can be an estimate of the glass transition temperature of the material. The printed neat PEEK displays a peak of its loss modulus near 133 °C, indicating a slightly lower temperature value than reported in literature [21]. The annealed, printed PEEK exhibits a loss modulus that is lower in value than the printed PEEK, while maintaining a higher T_g at approximately 147 °C. A higher

glass transition temperature is often associated with a higher degree of crystallinity, as the rigid crystallites within the polymer require more energy, in the form of heat, to transition from the glassy state to the rubbery state. However, as an amorphous material, the S-PEEK shows a much higher loss modulus, indicating that there is more energy dissipated as heat, which is confirmed by the thermal degradation behavior that was seen in the TGA testing. Furthermore, the loss modulus for S-PEEK is at a much lower temperature, near 106 °C, which can preclude the material from use in environments with elevated temperatures. The Li-PEEK on the other hand, shows no loss modulus peak in the temperature range tested.

Figure 5c shows the tanδ of the materials, calculated as a ratio of the loss modulus to the storage modulus, which suggests the damping of the material itself, or the material's capacity to dissipate energy. The S-PEEK has the highest tanδ value of the PEEK samples tested, though it is at a lower temperature, implying that its damping properties are limited to more ambient temperatures. On the other hand, the Li-PEEK shows a low capacity to dissipate energy but maintains this value throughout. This suggests that it does not have a T_g indicated via the tanδ curve, but it maintains its properties throughout the heating cycle, as seen in the moduli discussed previously.

Lastly, the complex modulus, which is a measure of the material's stiffness based on the storage and loss moduli, reflects the trends seen in the storage modulus (**Figure 5d**). The neat PEEK exhibits a nearly consistent complex modulus until it's T_g, with the annealed PEEK showing similar behavior but extended to a higher temperature than the T_g of neat PEEK. The Li-PEEK keeps a complex modulus between 800 and 900 MPa from ambient temperature to 175 °C, suggesting that it maintains its stiffness despite any rise in temperatures. At ambient temperatures, the S-PEEK has the highest complex modulus, suggesting that it possesses the highest stiffness of the materials evaluated, but transitions to the rubbery state with a lower complex modulus sooner than its counterparts, exhibiting its limitations at elevated temperature. The thermomechanical properties investigated here demonstrate the importance of the lithiation procedure, not only to impart ionic conductivity, but also to provide thermal stability and mechanical stiffness at elevated temperatures.

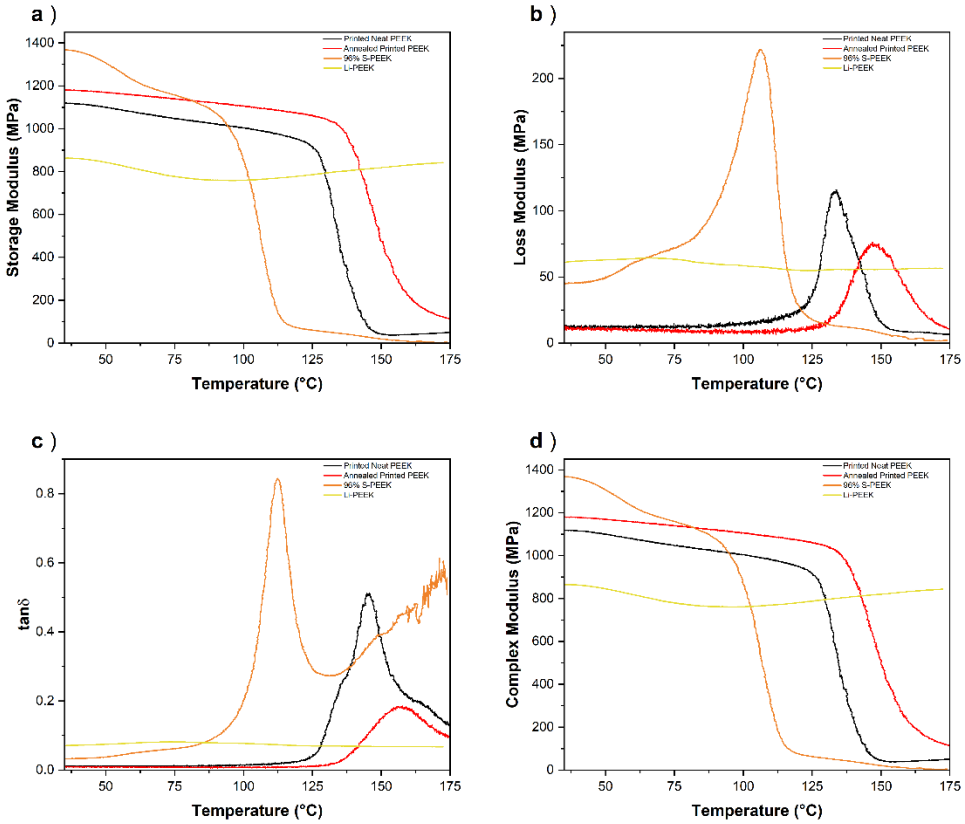

Figure 5*: Thermomechanical properties of 3D printed neat peak, annealed PEEK, sulfonated PEEK (S-PEEK), and lithiated PEEK (Li-PEEK) showing properties of* ***a)*** *storage modulus,* ***b)*** *loss modulus,* ***c)*** *tanδ, and* ***d)*** *complex modulus at temperatures ranging from ambient to 175 °C. All experiments were performed in air under a constant frequency of 1 Hz and an oscillating amplitude of 5 µm.*

3.2 Two-Phase Solid PEEK Electrolyte

Based on the properties of each PEEK constituent phase, a dual phase solid electrolyte, containing both amorphous and crystalline morphologies was hypothesized to create an optimized blend of properties. This dual phase electrolyte was achieved using FFF printed, neat PEEK disks that were surface sulfonated and lithiated according to the procedures mentioned previously in sections 2.2 and 2.3. By functionalizing only the outer surfaces of the PEEK, the material would act as the separator for the battery cell as well as the ionically conductive electrolyte and structural component, which had not been explored in literature at the time of publishing. This is partly enabled by the careful tailoring of the morphology through the functionalization process, where the core of the solid electrolyte remains semicrystalline, while the surface area becomes amorphous following sulfonation and lithiation treatments. A schematic of this dual phase morphology is provided in **Figure 6**. To characterize the properties of this novel, dual phase PEEK electrolyte, a series of morphological and elemental analyses were utilized before initial electrochemical characterization was completed.

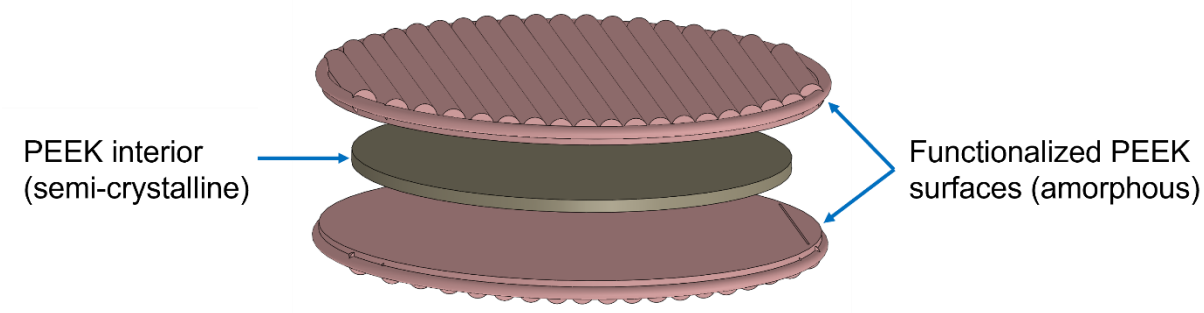

Figure 6: *Schematic of surface sulfonated PEEK electrolyte, featuring a semi-crystalline interior that is as-printed neat PEEK with amorphous, functionalized PEEK surfaces. The dual phase PEEK electrolyte aims to provide multifunctionality with ionic conductivity in the amorphous phase and stiffness in the semi-crystalline phase.*

3.2.1 Morphological Properties

As described in previous wide-angle and medium-angle x-ray scattering (WAXS/MAXS) studies, the crystalline behavior of neat PEEK that has been printed and annealed displays distinct crystalline peaks at 110, 111, 200, and 211 peaks. Once the neat PEEK has been functionalized via the complete sulfonation, the semicrystalline nature of the morphology is instead replaced by an amorphous phase, devoid of crystalline peaks. To achieve a dual phase PEEK electrolyte, which features both crystalline and amorphous regions at the center and surfaces, respectively, a surface sulfonation technique was used. By targeting the surfaces of the solid polymer electrolyte, the necessary amorphous morphology can be enabled for ionic conductivity while maintaining the crystalline phase in the center of the electrolyte to serve the purposes of adding stiffness and structure while acting as a separator between the two electrodes. The crystalline "separator" prevents short circuiting from the anode and cathode materials coming into contact, and acts as a preventative measure in the case of lithium dendrites forming and piercing through the separator. Since lithium dendrites are often a source of lithium-ion battery failure, the addition of the solid electrolyte serves a multifunctional purpose while increasing the potential safety factor of the cell.

In order to preliminarily quantify the dual phase architecture that is constructed via FFF and surface sulfonation methods, WAXS was utilized to observe the morphology through the thickness of the PEEK samples. **Figure 7** displays the WAXS curves for neat PEEK, sulfonated PEEK, and the dual phase, surface sulfonated PEEK. It is observed that the surface sulfonated electrolyte displayed both crystalline and amorphous behavior, acting as an intermediate between the functionalized and nonfunctionalized phases. The crystalline peaks in the surface sulfonated PEEK show a lower normalized intensity compared to the printed neat PEEK, suggesting that there is a lower degree of crystallinity, attributed to the enabled amorphous phase on the surfaces of the sample.

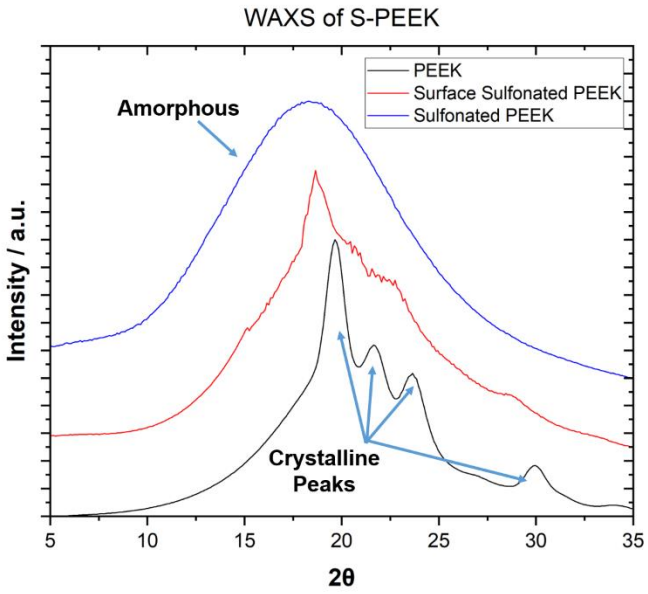

***Figure 7**: Wide angle x-ray scattering (WAXS) reduced 1D scattering data of neat PEEK, sulfonated PEEK, and surface sulfonated PEEK. Surface sulfonated PEEK electrolyte comprises dual phases of amorphicity and crystallinity within its structure, represented in the figure with fewer crystalline peaks than its neat counterpart.*

3.2.2 Microbeam and X-Ray Fluorescence of Sulfonated PEEK

The surface sulfonated samples were examined further at the Functional Materials Beamline (FMB) using WAXS and x-ray fluorescence (XRF) detectors at the beamline. Building off the 1D scattering data in **Figure 7**, a crystallinity index map of the cross-section of surface sulfonated samples was constructed from WAXS detector images. This map alongside a sulfur map created from XRF detector images of the same cross-sectional area allowed for an in-depth understanding of the role of functionalization on the morphology. The resultant maps can be found in **Figure 8**, with a schematic of the printed, surface sulfonated sample for orientation on the maps of crystallinity index and sulfur-XRF.

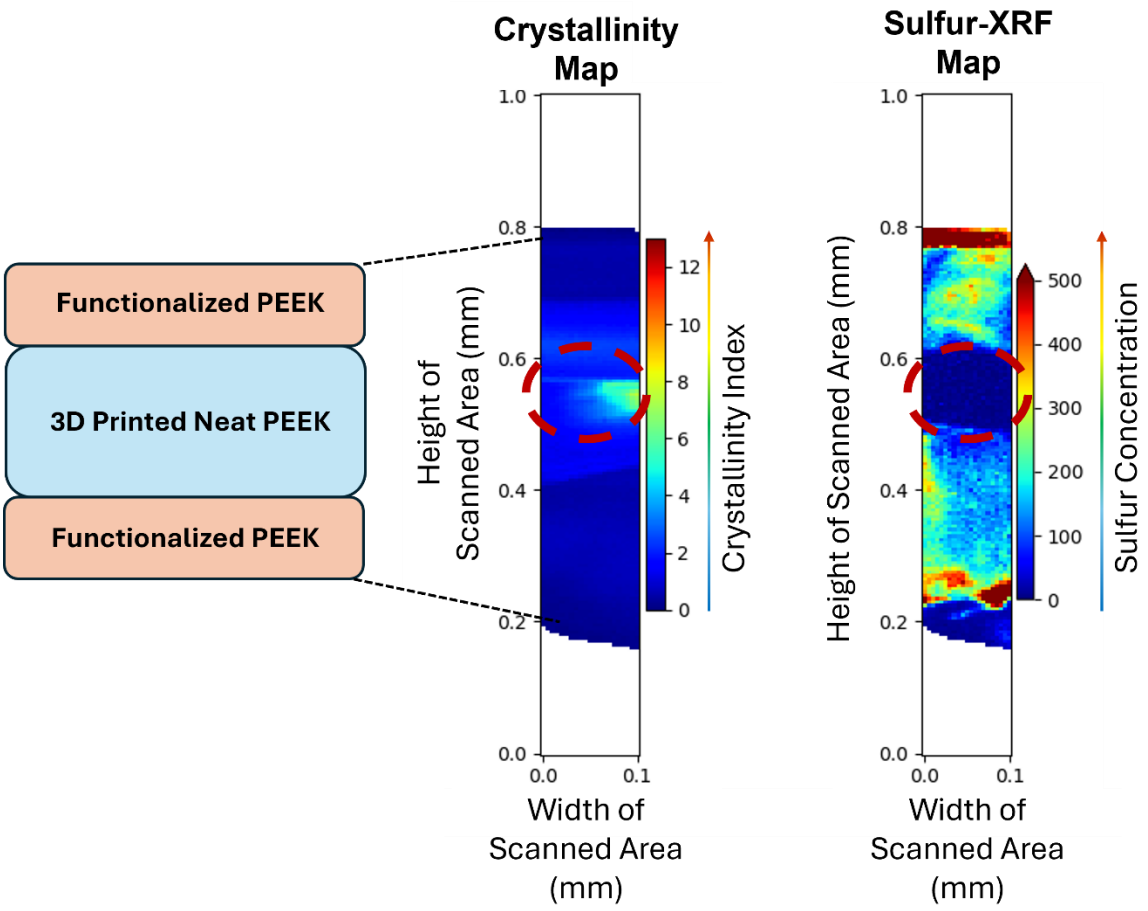

Figure 8: *Wide angle x-ray scattering derived map of crystallinity index and corresponding sulfur x-ray fluorescence maps illustrating the correlation between crystallinity and areas of electrolyte that have been exposed to sulfonation treatment.*

Prior to functionalization, the printed PEEK sample exhibited a gradient in crystallinity index, with the highest level of crystallinity near the print bed, where the material was thermally insulated and allowed for the polymer chains to assemble into crystallites. As shown in **Figure 8**, following the sulfonation treatment, the two surfaces of the printed PEEK electrolyte have a crystallinity index of 0, indicating that these areas are in fact, amorphous. In the center of the printed piece, the crystalline index increases, displaying a crystalline phase in the center of the sample's thickness. When compared to the sulfur-XRF map, there is a clear correlation between the depth of sulfur atoms detected to the amorphous regions depicted in the crystallinity index map. The highest concentration of sulfur is found on the top and bottom surfaces of the electrolyte, where the PEEK was in direct contact with the sulfuric acid during treatment. The concentration of sulfur gradually decreases with distance from the surface, leaving a center area that does not have any sulfur that was detected via the XRF technique. The sulfur-free area directly corresponds to the semicrystalline region of the electrolyte, implying that the amorphous and crystalline phases can not only coexist, but can be carefully tailored to defined regions of the polymer structure to allow for optimized properties.

4. CONCLUSIONS

The results presented in this study suggest that functionalizing PEEK through means of sulfonation and subsequent lithiation processes can provide ionic conductivity to enable its use as solid polymer electrolyte in structural battery composites. It was found that these processes enable an amorphous morphology in the polymer, which is conducive for conducting ions, while demonstrating the ability to remain thermally stable at elevated temperatures. Furthermore, the use of these functionalization techniques can be applied to specific areas of the PEEK electrolyte, allowing for a two-phase architecture to act as both an amorphous energy storage component and a semicrystalline strength component. With the foundational understanding of functionalizing PEEK for ionic conductivity and the ability to further tailor its morphology, future work aims to integrate these materials into additive manufacturing feedstocks that can be used to print mesh electrolyte structures that provide both strength and energy storage capabilities more efficiently. Ultimately, the findings in this work and the promise of future optimization of PEEK solid electrolytes demonstrate the potential to overcome the limitations of traditional liquid electrolytes and enable the next generation of structural battery technologies.

5. REFERENCES

1. M. Li, J. Lu, Z. Chen, and K. Amine, *30 Years of Lithium-Ion Batteries*. Volume 30, Issue 33. Advanced Materials: Wiley, 2018. DOI: https://doi.org/10.1002/adma.201800561
2. L. Asp, K. Bouton, D. Carlstedt, S. Duan, R.Harnden, W. Johannisson, M. Johansen, M. K. G. Johansson, G. Lindbergh, F. Liu, K. Peuvot, L. M. Schneider, J. Xu, and D. Zenkert, A Structural Battery and its Multifunctional Performance. Volume 2, Issue 3. Advanced Energy and Sustainability Research: Wiley, 2021 DOI: https://doi.org/10.1002/aesr.202000093
3. J. Snyder, R. Carter, and E. Wetzel, *Electrochemical and Mechanical Behavior in Mechanically Robust Solid Polymer Electrolytes for Use in Multifunctional Structural Batteries*. Volume 19, Issue 15. Chemistry of Materials: ACS Publications, 2007. DOI: https://doi.org/10.1021/cm070213o
4. J. Xu, Z. Geng, M. Johansen, D. Carlstedt, S. Duan, T. Thiringer, F. Liu, and L. Asp, *A multicell structural battery composite laminate*. Volume 4, Issue 3. EcoMat: Wiley, 2022. DOI: https://doi.org/10.1002/eom2.12180
5. K. Moyer, C. Meng, B. Marshall, O. Assal, J. Eaves, D. Perez, R. Karkkainen, L. Roberson, and C. L. Pint, *Carbon fiber reinforced structural lithium-ion battery composite: Multifunctional power integration for CubeSats*. Volume 24. Energy Storage Materials: Elsevier, 2020. DOI: https://doi.org/10.1016/j.ensm.2019.08.003
6. W. Huang, P. Wang, X. Liao, Y. Chen, J. Borovilas, T. Jin, A. Li, Q. Cheng, Y. Zhang, H. Zhai, A. Chitu, Z. Shan, and Y. Yang, *Mechanically-robust structural lithium-sulfur battery with high energy density*. Volume 33. Energy Storage Materials: Elsevier, 2020. DOI: https://doi.org/10.1016/j.ensm.2020.08.018
7. Y. Miao, P. Hynan, A. von Jouanne, and A. Yokochi, *Current Li-Ion Battery Technologies in Electric Vehicles and Opportunities for Advancements*. Volume 12, Issue 6. Energies: MDPI, 2019. DOI: https://doi.org/10.3390/en12061074

8. J. Fergus, *Ceramic and polymeric solid electrolytes for lithium-ion batteries*. Volume, 195, Issue 15. Journal of Power Sources: Elsevier, 2010. DOI: https://doi.org/10.1016/j.jpowsour.2010.01.076
9. F. Gucci, M. Grasso, C. Shaw, G. Leighton, V. Marchante Rodriguez, and J. Brighton, *PEO-based polymer blend electrolyte for composite structural battery*. Volume 62, Issue 8. Polymer-Plastics Technology and Materials: Taylor & Francis, 2023. DOI: https://doi.org/10.1080/25740881.2023.2180391
10. T.E. Attwood, P.C. Dawson, J.L. Freeman, L.R.J. Hoy, J.B. Rose, and P.A. Staniland, *Synthesis and properties of polyaryletherketones*. Volume 22, Issue 8. Polymer: Elsevier, 1981. DOI: https://doi.org/10.1016/0032-3861(81)90299-8
11. J.C. Seferis, *Polyetheretherketone (PEEK): Processing-structure and properties studies for a matrix in high performance composites*. Volume 7, Issue 3. Polymer Composites: Wiley, 1986. DOI: https://doi.org/10.1002/pc.750070305
12. T. Yap, N. Heathman, B. Shirani Bibabadi, E. Motta de Castro, A. Tamijani, A. Asadi, and M. Tehrani, *In-plane properties of an in-situ consolidated automated fiber placement thermoplastic composite*. Volume 188. Composites Part A: Applied Science and Manufacturing, 2025. DOI: https://doi.org/10.1016/j.compositesa.2024.108525
13. Y. Qin, G. Ge, J. Yun, X. Tian, X. Liu, J. Han, and S. Gao, *Enhanced impregnation behavior and interfacial bonding in CF.PEEK prepreg filaments for 3D printing application*. Volume 20. Journal of Materials Research and Technology: Elsevier, 2022. DOI: https://doi.org/10.1016/j.jmrt.2022.09.005
14. B.J. Ree, B. Zheng, A. Abbott, L. M. Smieska, A. R. Woll, Z. Renwick, and H. Koerner, *Mapping Crystallization Kinetics during 3D Printing of Poly(ether ether ketone).* Volume 57, Issue 6. Macromolecules: ACS Publications, 2024. DOI: https://doi.org/10.1021/acs.macromol.3c02327
15. M. Carrola, H. Fallahi, H. Koerner, L.M. Perez, and A. Asadi, *Fundamentals of crystalline evolution and properties of carbon nanotube-reinforced polyether ether ketone nanocomposites in fused filament fabrication*. Volume 15, Issue 18. ACS Applied Materials & Interfaces: ACS Publications, 2023. DOI: https://doi.org/10.1021/acsami.3c01307
16. B. Shirani Bibabadi, E. Motta de Castro, M. Carrola. P. Koirala, M. Tehrani, and A. Asadi, *Engineering the Crystalline Architecture for Enhanced Properties in Fast-Rate Processing of Poly (ether ether ketone) (PEEK) Nanocomposites*. Volume 2, Issue 8. ACS Applied Engineering Materials: ACS Publications, 2024. DOI: https://doi.org/10.1021/acsaenm.4c00217
17. N.R. Enos, O.D. McNair, and J.S. Wiggins, *The Influence of Carbon Fiber on Crystallization and Morphology of Poly(Ether Ketone Ketone) Composites Towards High Rate Thermoplastic Manufacturing Processes*. Volume 60, Issue 6. SAMPE Journal: SAMPE. DOI: 10.33599/SJ.v60no6.02
18. L. Li, R. Xiong, X. Wang, M. Zhou, S. Sun, G. Shen, L. Song, Y. Zhang, and H. Zhou, *Lithiated poly(ether ether ketone) separators with excellent thermal stability and*

electrolyte wettability for lithium-ion battery. Volume 57. Journal of Materials Science: Springer, 2022. DOI: https://doi.org/10.1007/s10853-022-07761-0

19. L. Smieska, R. Mullett, L. Ferri, and A.R. Woll, *Trace elements in natural azurite pigments found in illuminated manuscript leaves investigated by synchrotron x-ray fluorescence spectroscopy and diffraction mapping*. Volume 123. Applied Physics A: Springer, 2017. DOI: https://doi.org/10.1007/s00339-017-1093-0
20. S. Banerjee and K.K. Kar, *Impact of degree of sulfonation on microstructure, thermal, thermomechanical and physicochemical properties of sulfonated poly ether ether ketone*. Volume 109. Polymer: Elsevier, 2017. DOI: https://doi.org/10.1016/j.polymer.2016.12.030
21. G. Liu, N. Hu, J. Huang, Q. Tu, and F. Xu, *Experimental Investigation on the Mechanical and Dynamic Thermomechanical Properties of Polyether Ether Ketone Based on Fused Deposition Modelling*. Volume 16, Issue 21. Polymers: MDPI, 2024. DOI: https://doi.org/10.3390/polym16213007